Structure Formation and Tearing of an MeV Cylindrical Electron Beam in a Laser-Produced Plasma

Toshihiro Taguchi,[1] Thomas M. Antonsen, Jr.,[2] Chuan S. Liu,[2] and Kunioki Mima[3]
[1]*Department of Electrical Engineering, Setsunan University, Neyagawa, Osaka, Japan*
[2]*Institute for Plasma Research, University of Maryland, College Park, Maryland 20742*
[3]*Institute of Laser Engineering, Osaka University, Suita, Osaka, Japan*
(Received 23 October 2000)

The stability of a cylindrical, solid hot electron beam propagating in a high density plasma has been studied using a two-dimensional, hybrid Darwin code. The initially solid beam evolves into a hollow, annular beam due to the Weibel instability and generates strong magnetic fields on both sides of the annular ring. The annular structure subsequently breaks up into several beamlets via a mechanism similar to a tearing instability. It is found that the magnetic fields parallel to the direction of beam propagation also grow due to the tearing process.

DOI: 10.1103/PhysRevLett.86.5055 PACS numbers: 52.35.Py, 52.40.Mj, 52.65.Kj

Ultraintense, short pulse lasers [1,2] have been developed in recent years to generate relativistic plasmas. When the irradiation intensity approaches 10^{18} W/cm^2, the electron quiver velocity is close to the speed of light. Near the cutoff surface, where the plasma frequency equals the laser frequency, the laser generates an intense relativistic electron stream which carries the absorbed laser energy into the overdense plasma. The electric current associated with the electron stream reaches 100 MA or higher in a diameter of a few tens of micrometers when the input laser power is 100 TW or higher. Since the relativistic electron current is much higher than the Alfvén limiting current, $\gamma m_e c^3/e \simeq 17\gamma$ kA for a relativistic electron beam with average energy of $(\gamma - 1)m_e c^2$, the relativistic electron current penetrating into the overdense plasma will be neutralized by a return current induced in the background. Through this process, the absorbed laser energy is transported into the dense plasma. Further, this process has significant consequences for the fast ignition concept [3] of the laser fusion research.

Although the return current carried by thermal background electrons removes the Alfvén current limitation, the resulting bi-Maxwellian electron distribution is susceptible to a number of instabilities, including the Weibel instability [4,5]. The Weibel instability is characterized by the variation of perturbed quantities in the direction transverse to the beam axis. It generates strong magnetic fields transverse to the direction of beam propagation, and the magnetic field causes the beam to break up and be deflected.

The electromagnetic dynamics of relativistic electrons generated by ultraintense lasers has been widely studied by computer simulation [6–10]. Many of the studies use electromagnetic, particle-in-cell (PIC) codes, which can describe kinetic effects of hot electrons and full electromagnetic processes. However, 2D or 3D PIC codes require large computer memory because they usually use a few tens of particles per computational grid to reduce statistical fluctuations. PIC codes also consume computer CPU time because they must use small time steps, which are limited by the Courant condition, $c\Delta t/\Delta \leq 1$, where Δt is the time step, Δ is the grid spacing, and c is the speed of light. The grid spacing in PIC codes must be the order of the Debye length λ_D [11], then the time step is shorter than $v_{te}/(c\omega_{pe})$, where v_{te} is the thermal velocity of the electrons, and ω_{pe} is the electron plasma frequency.

In order to reduce computational time and memory consumption and to simulate large scale plasmas for long time durations, we have developed a new type of simulation code, a hybrid Darwin code. This code has two features. The first is that it uses a hybrid description, i.e., hot electrons and cold electrons are separately described. Hot electrons, whose density is lower, are described as particles, while cold electrons, whose density is higher, are described as a fluid. Since the hot electron density is approximately of the order of the cutoff density, the density of cold electrons, which is approximately the same as the background density, is always much higher than the hot electron density in overdense plasmas. While the particle treatment retains the kinetic effects of hot electrons, the fluid description of cold electrons enables us to reduce the total amount of memory consumption. The cold electron quantities, such as density or velocity, are assigned only on the computational grids, which are several times fewer in number than the particles. This feature is especially important for the analysis of hot electron dynamics in very high density plasmas.

The other feature of our code is that it uses the Darwin approximation to calculate the self-consistent electromagnetic fields [12]. This approximation extends the electron magnetohydrodynamics (EMHD) model [13,14] to include space charge effects. In the Darwin approximation, the electric field $\boldsymbol{E}$ is divided into a divergence-free component $\boldsymbol{E}_T$, where $\nabla \cdot \boldsymbol{E}_T = 0$, and a curl-free component $\boldsymbol{E}_L$, where $\nabla \times \boldsymbol{E}_L = 0$. The displacement current due to the divergence-free component is neglected. Since both components of the electric field in the Darwin approximation are calculated directly by either Helmholtz or Poisson equations, it is not necessary to solve for the

temporal evolution of the electric fields. As a result, high frequency oscillations such as high frequency electromagnetic waves are automatically removed, and the restriction, $c\Delta t/\Delta \lesssim 1$, is not necessary. Since this model includes self-consistent electrostatic fields, the time step is usually shorter than $1/\omega_{pe}$. This time step is longer than the time step of PIC codes ($c\Delta t \le \Delta \le v_{tc}/\omega_{pe}$) by the ratio of c/v_{tc}, where v_{tc} is the thermal velocity of cold electrons. Since we also have no constraint that the grid size must be of the order of λ_D, we can take it to be a fraction of the collisionless skin depth, c/ω_{pe}, which is usually larger than $\lambda_D = v_{tc}/\omega_{pe}$ in cold plasmas. These advantages enable us to do large scale simulations for the hot electron dynamics in cold overdense plasmas.

We have performed two-dimensional simulations using the hybrid Darwin code to analyze the evolution of an initially solid cylindrical, hot electron beam propagating in an overdense plasma. In the simulations, vector quantities retain all three components; however, spatial variation is restricted to the two directions (x, y) transverse to the direction of beam propagation. Recently, Honda *et al.* showed simulation results for such a case using a PIC code [9,10]. Since they, however, assumed a uniform beam initially, they did not simulate the macroscopic dynamics of beam structure formation that we consider here.

Figures 1–3 show the results. Figures 1(a) and 1(b) are the hot electron density profile at different times, $\omega_{pe}t =$ (a) 67 and (b) 81, where $\omega_{pe}^2 = 4\pi e^2 n_0/m_e$, which is determined by the background ion density n_0. These times are sufficiently short that ions can be taken to be immobile as we have assumed. The initial hot electron beam profile is cylindrically flattop, and its diameter is 200Δ, where Δ is the grid spacing. The peak hot electron density is set to be $0.1n_0$, while the initial cold electron density is determined to maintain charge neutrality. In the figure, the density is normalized by n_0. The total simulation system is $512\Delta \times 512\Delta$, while we show only the central region of size $120\Delta \times 120\Delta$ where the beam pinches. The normalized collisionless skin depth $c/(\omega_{pe}\Delta) = 8$ in the simulation. The initial average velocity of the hot electrons $\langle v_z \rangle$ is $0.885c$ (Lorentz factor $\gamma_0 = 2.15$), and the initial flow velocity of the cold electrons u_{cz} is set so as to cancel the initial hot electron current ($n_h\langle v_z \rangle + n_c u_{cz} = 0$).

The dimensionless parameters of the simulation correspond to dimensional parameters as follows. When $n_0 = 10^{22}$ cm^{-3}, $\omega_{pe}^{-1} = 0.177$ fs and $\Delta = 6.64 \times 10^{-3}$ μm, and, hence, the diameter of the hot electron beam is about 1.33 μm. Figures 1(a) and 1(b) show the results at times corresponding to 11.9 and 14.4 fs, respectively. The initial temperatures of both hot and cold electrons are set to be 5 keV.

As shown in Fig. 1(a), the density of the circular edge of the hot electron beam increases, and the beam gradually forms an annulus. This is due to the Weibel instability. When the temperatures of hot and cold electrons are

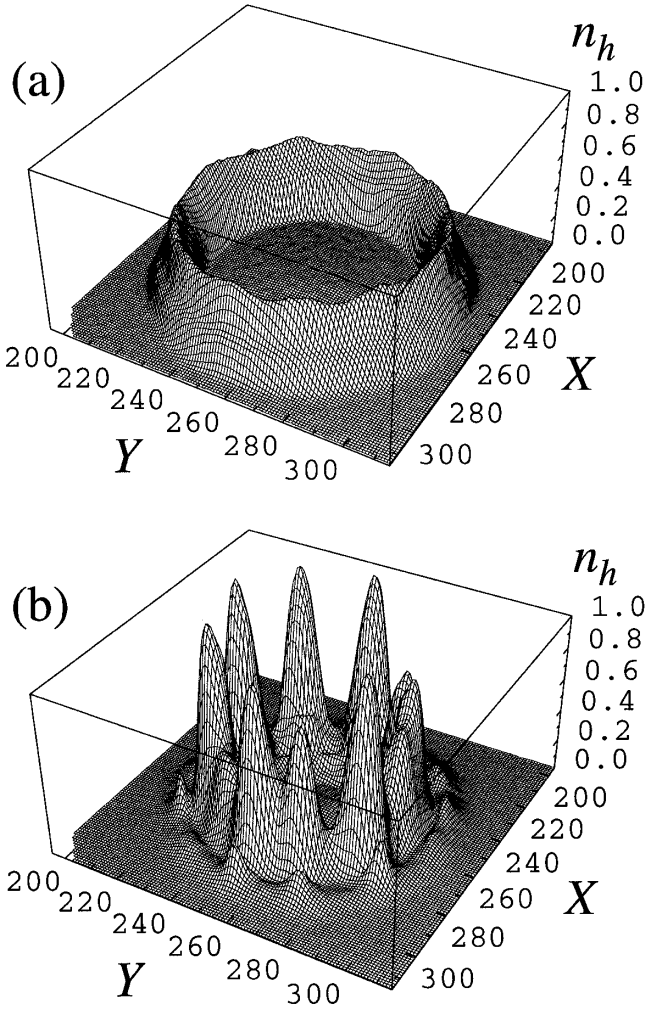

FIG. 1. Temporal evolution of hot electron density profile, $n_h(x, y)$, at $\omega_{pe}t =$ (a) 67 and (b) 81.

equal, the growth rate of the Weibel instability Γ_W for the relativistic case is described by the following formula [8]:

$$\Gamma_W = \left[\frac{\alpha n_{h0} u_{h0}^2/n_{c0}}{\beta + c^2k^2/\omega_{pe}^2} - c_{h0}^2 \right]^{1/2} k . \qquad (1)$$

Here, n_{h0} and n_{c0} are the initial densities of hot and cold electrons, respectively, u_{h0} is the initial flow velocity of hot electrons, $c_{h0} = (\mu_h T_{h0}/m_e\gamma_0)^{1/2}$ is the thermal velocity of hot electrons, where μ_h is the adiabatic constant, T_{h0} is the initial temperature of hot electrons, and k is the wave number of the unstable mode. The quantities $\alpha = (n_{c0}/\gamma_0 + n_{h0})/n_0$ and $\beta = (n_{h0}/\gamma_0 + n_{c0})/n_0$ are relativistic correction factors. The growth rate has a maximum at $c^2k_{\max}^2/\omega_{pe}^2 = (\alpha\beta n_{h0}u_{h0}^2/n_{c0}c_{h0}^2)^{1/2} - \beta$. For the parameters of the simulation, $n_{h0}/n_{c0} = \frac{1}{9}$, $u_{h0}/c = 0.885$ ($\gamma_0 = 2.15$), and $c_{h0}/c = 0.0871$ for $\mu_h = \frac{5}{3}$, the wave number satisfies $ck_{\max}/\omega_{pe} = 1.19$, and the wavelength for maximum growth is about 42 grids. This is approximately twice the annular beam thickness. The initial cylindrical beam is radially inhomogeneous. For this

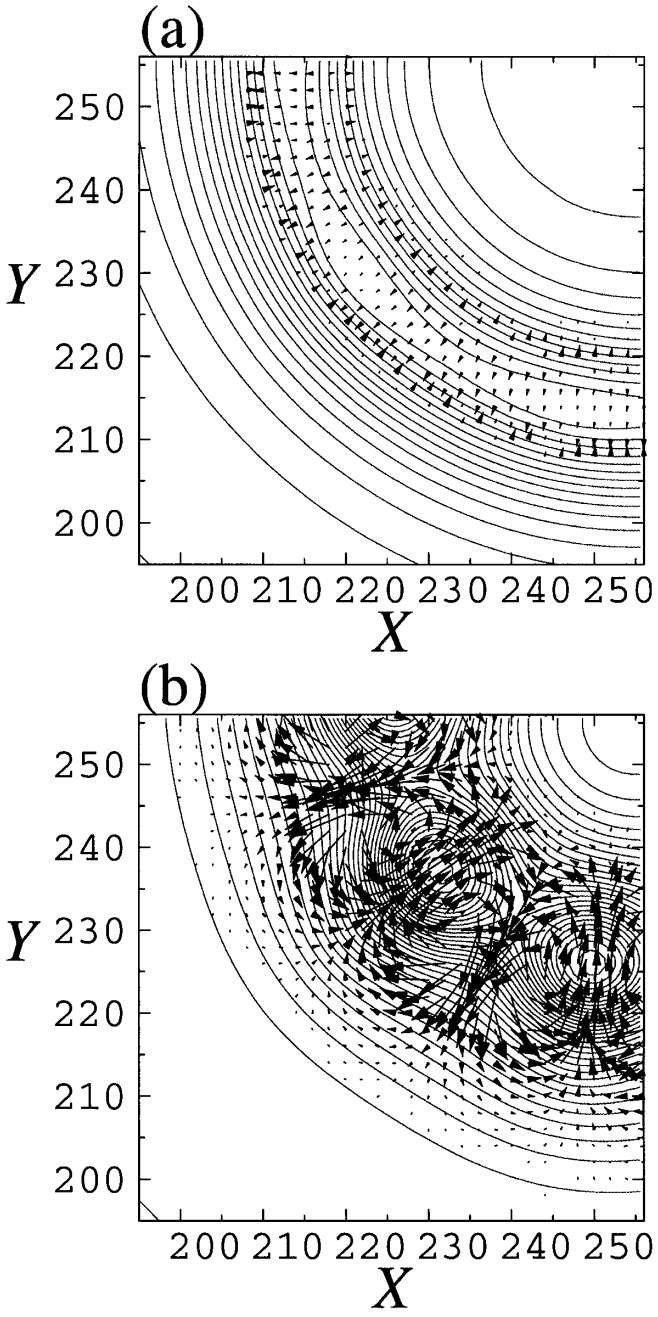

FIG. 2. Temporal evolution of magnetic field lines at $\omega_{pe}t =$ (a) 67 and (b) 81. The arrows in the figures show total electron fluxes $n_c\boldsymbol{u}_c + n_h\langle\boldsymbol{v}\rangle$.

reason, the first perturbations to grow have no azimuthal variation. However, as shown in Figs. 1(a) and 1(b), the annular beam gradually pinches, becomes unstable, develops azimuthal structure, and breaks up into several narrow filaments. Since each narrow beam of hot electrons carries a current, the narrow beams attract each other, and they eventually coalesce into a single hot electron beam at about $\omega_{pe}t = 140$. The process of coalescence is similar to the results of Honda *et al.* [9,10]. We have also simulated the case of a beam that initially has a smooth Gaussian dependence on radius. In this case, the beam also develops an annular structure first before breaking into filaments.

Figures 2(a) and 2(b) show isocontours of the z component of the vector potential A_z, which correspond to magnetic field lines in the 2D case. The plots correspond to the same times as in Figs. 1(a) and 1(b). Figure 2(a) shows that the magnetic field is generated on both the inside and the outside of the annular beam. Further, the field lines reconnect as the beam breaks up into several narrow beams, as shown in Figs. 2(a) and 2(b). This process is very similar to the tearing instability in magnetized plasmas.

Since ions are immobile and only electrons participate, the process is closely related to whistler mediated magnetic reconnection, which was proposed by Mandt *et al.* [15]. Whistler mediated reconnection is characterized by the generation of an out-of-plane magnetic field, which is transverse to the original magnetic field generated by the current sheet. Under the current conditions, the generation of the out-of-plane field implies the generation of a magnetic field parallel to the direction of beam propagation.

The arrows in Fig. 2 show the total electron flux vectors, $n_h\langle\boldsymbol{v}_\perp\rangle + n_c\boldsymbol{u}_{c\perp}$, which are proportional to the current density. The vectors clearly indicate the presence of current loops in the plane after the tearing is well developed. The loops generate the out-of-plane magnetic field. Figure 3 shows the temporal evolution of the maximum strength of the in-plane magnetic field. Figure 3 shows the temporal evolution of the maximum strength of the in-plane magnetic field, B_T, and the out-of-plane magnetic field, B_z, respectively. In the figure, the magnetic field is normalized by $B_0 = (4\pi n_0 T_{h0})^{1/2}$, where $B_0 = 31.7$ MG for the current parameters. The figure shows that the out-of-plane field grows exponentially after the tearing process becomes significant. The maximum in-plane magnetic field is about 80 MG for the current parameters, while the maximum out-of-plane field reaches about 28 MG.

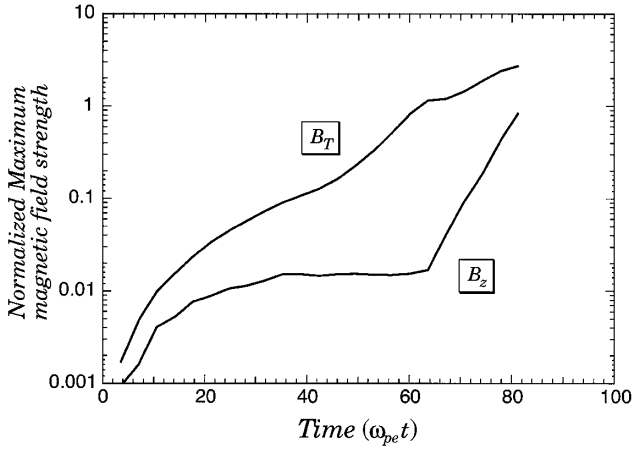

FIG. 3. Maximum magnetic field strength in the simulation region. Here, B_T is the transverse component to the beam propagation, and B_z is the parallel components to it.

There is a major difference between pure whistler mediated reconnection and our results. While whistler reconnection generates a quadrupole out-of-plane field around the X point [16], our results show a dipole field, which changes sign on both sides of the X point. The dipole field appears because the hot electron beam has an inward velocity due to the pinch. From our simulation results [Figs. 2(a) and 2(b)], the inward velocity is estimated as about $u_{h\perp} \simeq 0.1c$. On the other hand, the background electrons do not have such a large radial velocity component, although their density n_c changes as it neutralizes the hot electron density. As a result, the hot electrons and the cold electrons have a relative radial flow. When the beam has cylindrical symmetry, the relative flow does not contribute to the generation of an out-of-plane magnetic field. But as the tearing develops, the hot electron flow and the cold electron flow in the plane are also torn, and this produces a current loop with opposite sign on either side of the X point. According to this process, the generated magnetic field is estimated as $(B_0/2)[\Delta L/(c/\omega_{pe})](n_h/n_0)(u_{h\perp}/v_{th0})$, where ΔL is the size of the narrow beam, and $v_{th0} = (T_{h0}/m_e)^{1/2}$. For the current parameters, $n_h \simeq n_0$, $v_{th0} = 0.099c$, and $\Delta L \simeq 15\Delta \simeq 2c/\omega_{pe}$, the value is about B_0, which agrees well with the maximum strength of B_z. In our simulation, the quadrupole field is too small to be observed.

In conclusion, we have studied the stability of hot electron transport and strong magnetic field generation in overdense plasmas, which is critically important for the fast ignition concept. For this purpose, we have used a newly developed hybrid Darwin code. The results show that the cylindrical hot electron beam, which is initially solid, gradually forms annular structure due to the Weibel instability, and the annular ring breaks up into several narrow beams through a similar process to a tearing instability. The tearing process is accompanied by the generation of an out-of-plane magnetic field. The out-of-plane field in our simulation had a dipole character, which can be explained by the relative velocity between the hot and the cold electron flows in the transverse plane. Since the out-of-plane field reaches a strength on the same order of the in-plane field, the three-dimensional field lines form spirals as they surround the hot electron beam.

A hybrid description has a potential to reduce the memory consumption for the simulation of a much higher density region than the current one. While the major memory consumption of the PIC code comes from its usage of a large number of particles, a hybrid code uses particles only for the hot electrons, and then one particle per one grid is enough for such a high density region. This means that the total required memory is proportional to the number of grids assigned on fields such as a pure fluid code.

However, although our new code is more suitable for the analysis of a large area of overdense plasma than a PIC code, the limitation on the time step by $1/\omega_{pe}$ and on the grid size by the factor c/ω_{pe} is still tight for a very high density region ($\gtrsim 10^3$ critical density). Plasma oscillations are not expected to be so important in such overdense regions. This is because charge neutrality is well maintained in these regions, and the small electrostatic field will not affect the beam dynamics significantly. One possibility to relax the limitation of the time step is to use an implicit scheme in the temporal evolution. Using such a scheme and to use a few tens of gigabytes memory machine, the full scale simulation of the fast ignitor beam can be done.

One of the authors (T. T.) thanks M. A. Shay and B. N. Rogers of University of Maryland for help in developing our new simulation code. We also thank J. F. Drake for a number of fruitful discussions and comments. This work was supported by JIFT, and part of this work is supported by a grant-in-aid for scientific research from the Ministry of Education, Sports Culture, Science and Technology and by the National Science Foundation and the U.S. Department of Energy.

[1] D. Strickland and G. Mourou, Opt. Lett. **20**, 1157 (1995).
[2] P. Maine, D. Strickland, P. Bado, M. Pessot, and G. Mourou, IEEE J. Quantum Electron. **24**, 398 (1988).
[3] M. Tabak, J. Hammer, M. E. Glinsky, W. L. Kruer, S. C. Wilks, J. Woodworth, E. M. Campbell, M. D. Perry, and R. J. Mason, Phys. Plasmas **1**, 1626 (1994).
[4] E. S. Weibel, Phys. Rev. Lett. **2**, 83 (1959).
[5] F. Califano, F. Pegoraro, and S. V. Bulanov, Phys. Rev. E **56**, 963 (1997).
[6] R. J. Mason and M. Tabak, Phys. Rev. Lett. **80**, 524 (1998).
[7] A. Pukhov and J. Meyer-ter-Vehn, Phys. Rev. Lett. **79**, 2686 (1997).
[8] Y. Sentoku, K. Mima, S. Kojima, and H. Ruhl, Phys. Plasmas **7**, 689 (2000).
[9] M. Honda, J. Meyer-ter-Vehn, and A. Pukhov, Phys. Plasmas **7**, 1302 (2000).
[10] M. Honda, J. Meyer-ter-Vehn, and A. Pukhov, Phys. Rev. Lett. **85**, 2128 (2000).
[11] C. K. Birdsall and A. B. Langdon, *Plasma Physics via Computer Simulation* (McGraw-Hill, New York, 1985), p. 176.
[12] J. Busnardo-Neto, P. L. Pritchett, A. T. Lin, and J. M. Dawson, J. Comput. Phys. **23**, 300 (1977).
[13] A. S. Kingsep, K. V. Chukbar, and V. V. Yan'kov, in *Reviews of Plasma Physics,* edited by B. B. Kadomtsev (Consultants Bureau, London, 1990), Vol. 16, p. 243.
[14] S. V. Bulanov, F. Pegoraro, and A. S. Sakharov, Phys. Fluids B **4**, 2499 (1992).
[15] M. E. Mandt, R. E. Denton, and J. F. Drake, Geophys. Res. Lett. **21**, 73 (1994).
[16] M. A. Shay and J. F. Drake, Geophys. Res. Lett. **25**, 73 (1998).